JOURNAL OF AIRCRAFT
Vol. 45, No. 2, March–April 2008

Aerodynamics of Scaled Runback Ice Accretions

Edward A. Whalen,* Andy P. Broeren,† and Michael B. Bragg‡
University of Illinois at Urbana–Champaign, Urbana, Illinois 61801

DOI: 10.2514/1.32274

Runback ice accretions present a unique situation in iced-airfoil aerodynamics in that the airfoil typically has a clean leading edge before the ice accretion. To investigate the aerodynamic effects of runback ice accretions, simulations were scaled from accretions obtained in the NASA Glenn Icing Research Tunnel for testing in the Illinois subsonic wind tunnel. Simple geometric scaling, based on airfoil chord, as well as boundary-layer scaling, based on estimated boundary-layer thickness, was used. The NACA 3415 and the NACA 23012 airfoils were tested at a Reynolds number of 1.8×10^6 and Mach number of 0.18. Simple two-dimensional simulations were tested as well as three-dimensional simulations that more accurately simulated the features of the full-scale ice accretion. Significant aerodynamic penalties due to runback accretions were identified. In the worst case these penalties included a loss of over 0.75 in $C_{l\max}$ and 7 deg in stalling angle of attack. In certain cases scaled runback accretions were found to increase the stalling angle of attack and maximum-lift coefficient. This phenomenon was investigated using boundary-layer measurements and fluorescent-oil flow visualization. It was concluded that the interaction between the boundary layer and the simulation was responsible for the phenomenon.

Nomenclature

C_d	=	sectional drag coefficient
C_l	=	sectional lift coefficient
$C_{l\max}$	=	maximum section lift coefficient
C_m	=	sectional pitching moment
C_p	=	static pressure coefficient
c	=	model chord length
k	=	simulation height, ice thickness
n	=	surface normal coordinate
Re	=	Reynolds number
Re_k	=	Reynolds number based on obstacle height
T_s	=	static air temperature
T_0	=	total air temperature
U_∞	=	freestream wind-tunnel airspeed
u	=	local boundary-layer airspeed
x	=	chordwise coordinate
y	=	chordwise normal coordinate
α	=	angle of attack
α_{stall}	=	stalling angle of attack
δ	=	boundary-layer thickness

Introduction

RUNBACK ice accretions occur on surfaces equipped with thermal anti-icing systems when the system is not evaporating 100% of the water impinging on the surface. In this case the water runs back to the point where the added heat no longer raises the water film above its freezing temperature. The water begins to freeze, developing a ridge line and leaving the leading edge clean. In the case of hot-air systems, a portion of the bleed air from a turbine engine compressor is directed to a system that heats the leading-edge region of the wing using jets of the hot gas. More detailed information regarding this particular system can be found in Whalen et al. [1].

Runback icing is a potential problem in some phases of flight, for example, holding in icing and descent through icing conditions. Holding greatly increases the exposure time and can challenge the system during high water-catch rates or very low temperatures. The descent phase is also critical because the engine power is reduced and, therefore, less mass flow and lower temperature air is being provided to the system.

Data regarding the characteristics of runback ice accretions are relatively scarce compared to most other ice types such as those on unprotected surfaces and those resulting from pneumatic systems. Runback icing was investigated as early as 1953 when Gray and von Glahn [2] tested a NACA 65_1-212 airfoil equipped with a hot-air anti-icing system. The system was operated continuously, evaporating approximately 28 to 44% of the incoming water. They recorded the size and the location of the runback ridges and documented the accretion characteristics with photographs. In 2005, Whalen et al. [1] presented the results of a test program at the NASA Icing Research Tunnel to generate runback ice accretions on a full-scale model equipped with a hot-air anti-icing system running in a continuous mode. Ice accretions were generated at a number of flight and icing conditions considered critical to the effective operation of the hot-air system. Accretions from that test were documented with photographs, tracings, and castings.

Aerodynamic performance penalties of ice accretions are of particular concern for both the safety and certification of airplanes. In addition to generating runback ice accretions, Gray and von Glahn [2] also documented the drag penalties associated with the accretions. They documented significant drag penalties and noted that the most significant penalties were associated with those accretions nearest the leading edge. Studies by Jacobs [3], Lee and Bragg [4], and others have demonstrated the impact on aerodynamic performance of ice simulations similar in character to runback accretions. Lee and Bragg [4] studied ridge shapes using forward-facing quarter-round shapes and found dramatic losses in lift. In the worst case $C_{l\max}$ for the NACA 23012 was reduced to 0.27. In this research simulation heights of $k/c = 0.0083$ and 0.0139 were tested on a NACA 23012 and a NASA NLF (natural laminar flow) 0414 at x/c locations from $x/c = 0.0$ to 0.50. Jacobs placed a $k/c = 0.005$ spoiler at various chordwise positions on a 5-in. chord NACA 0012 at $Re = 3.1 \times 10^6$. His study was mostly concerned with the drag effects of manufacturing protuberances. He observed much more substantial reductions in $C_{l\max}$, from 1.51 to 0.8, for a $k/c = 0.005$ spoiler attached at $x/c = 5\%$ versus those attached at $x/c = 15\%$, where $C_{l\max}$ was reduced to approximately 1.31. Calay et al. [5]

Received 21 May 2007; revision received 8 October 2007; accepted for publication 11 October 2007.

*Graduate Research Assistant, Department of Aerospace Engineering. Member AIAA.

†Research Scientist, Department of Aerospace Engineering. Senior Member AIAA.

‡Professor, Department of Aerospace Engineering, Associate Dean for Research and Administrative Affairs. Fellow AIAA.

simulated runback ridges using a step, a ramp, and a triangular shape, each with $k/c = 0.0035$, on a NACA 0012 at $Re = 1.25 \times 10^6$ and found that the drag coefficient at 0-deg angle of attack increased by up to approximately 0.011 while $C_{l\max}$ decreased by up to 0.35 with the shapes at $x/c = 0.05$. He also found that the same simulations at $x/c = 15\%$ increased the $C_{l\max}$ of the airfoil. The greatest $C_{l\max}$ increase was approximately 0.08 and α_{stall} was delayed by 1 deg. Calay noted that the stall of the airfoil with the ice simulations began from the simulations rather than from the trailing edge, as was the case for the clean airfoil. He attributed the increase in $C_{l\max}$ to the flow remaining attached at greater angles of attack than in the clean case. The mechanism by which this occurred was not discussed except to say that the shape added "extra turbulence." Calay concluded that small changes in the ice configuration were able to produce large changes in the performance effect requiring accurate simulations to estimate actual runback effects. Papadakis and Gile-Laflin [6] also observed increases in airfoil performance due to a backward facing ramp with $k/c = 0.0041$ at $x/c = 15\%$ and a spoiler with $k/c = 0.0053$ at $x/c = 15\%$. Their tests were conducted using a modified NACA 63_A213 airfoil at $Re = 2.0 \times 10^6$. The ramp increased $C_{l\max}$ by 0.11 and delayed stall by 4 deg. The spoiler increased $C_{l\max}$ by 0.01 and delayed stall by 1 deg. Tests with the ramp at $x/c = 2.5\%$ reduced $C_{l\max}$ by 0.23 and the stalling angle of attack by 2 deg.

In addition to height and chordwise location, airfoil geometry can play a significant role in the effect of ice simulations on the aerodynamic performance of airfoils. Work by Lee and Bragg [7], Broeren and Bragg [8] and Broeren et al. [9] demonstrated this by testing identical simulations on multiple airfoil models. Of particular interest were the conclusions of Lee and Bragg [7] that stated that airfoils that were forward loaded, that is, with strong leading-edge suction peaks, were most susceptible to the effects of supercooled large droplet (SLD)-type ridges. This is because the ridges were positioned in regions of strong adverse pressure gradient, accentuating the effect of the ridge on the boundary layer.

Results for ridge-type shapes from Calay [5] and Papadakis [6] have demonstrated that accurate simulations of the ice accretions are required to estimate the penalties of runback accretions. Previous work by Broeren et al. [9] showed that geometric scaling of ice simulations based on the model chord was an accurate method to reproduce performance penalties in subscale tests. As part of that research, a forward-facing $k/c = 0.014$ quarter-round shape was used to simulate an SLD ridge at $x/c = 0.02$, 0.10, and 0.20. Performance penalties compared quite well across two scales (full and half) and a Reynolds number range from 1.8×10^6 to 10.5×10^6. This also demonstrated that the effects for those types of shapes were insensitive to the Reynolds number, a fact that had also been reported in other studies such as Lee and Bragg [7]. Results by Broeren and Bragg [8] reinforced the accuracy of geometric scaling and demonstrated the effectiveness of building up simulations from roughness elements. In that work, an intercycle ice accretion was simulated at subscale ($c = 1.5$ ft, $Re = 1.8 \times 10^6$) using layers of roughness elements and the performance effects were compared to those for the cast ice accretion at full scale ($c = 3.0$ ft, $Re = 2.0 \times 10^6$). The performance compared quite well and the method was adopted for a study of the role of airfoil geometry on the effects of those simulations.

Significant research has been conducted to understand the flow over two-dimensional fences, which are analogous to the ridge simulations used in icing research. Calay [5] concluded that the smallest ridge simulations he tested ($k/c = 0.0035$) interacted with the boundary layer to delay trailing-edge separation and increase the maximum-lift coefficient and stalling angle of attack. Schofield and Logan [10] showed that for fences with small k/δ, the separation zone aft of the shape was significantly shorter than in the case of large k/δ. This was a result of the relative length of the separation zone preceding the fences. In the small k/δ case the forward separation zone was longer in chordwise extent causing the slope of the separation streamline to be shallow and allowing the flow to reattach shortly aft of the fence. With large k/δ fences the separation zone forward of the fence was short in chordwise extent and the separation streamline had a steep slope that caused the streamlines around the shape to deflect significantly, delaying reattachment behind the fence to a point much farther downstream. In addition, devices such as fences [11] and spanwise cylinders [12] that generate transverse vortices have been shown to be effective in flow control applications. However, they are typically not as efficient as the more traditional wedge-type vortex generators that have been widely applied in flow control.

Aerodynamic penalty results for high-fidelity runback ice simulations, with the exception of the work by Gray and von Glahn [2], are nearly nonexistent. Although efforts have been made to simulate these accretions using low-fidelity simulations, no reference data exist for the penalties associated with these shapes. The objectives of this study were to measure the aerodynamic performance penalties of selected runback ice simulations and to investigate methods for the simulation and scaling of these shapes. This article reviews the aerodynamic testing of medium- and low-fidelity runback ice simulations on two airfoil geometries, the NACA 23012 and the NACA 3415, in the Illinois 3 ft $\times$ 4 ft subsonic wind tunnel at a Reynolds number of 1.8×10^6. The NACA 23012 was representative of the section used for the ice accretion testing and the NACA 3415 broadened the range of clean-airfoil characteristics. The medium-fidelity simulations were designed to capture some fine details of the ice accretion without employing an ice casting, which was not available for aerodynamic testing in the Illinois wind tunnel. The low-fidelity shapes were designed to capture the most significant effects of the ice shape with minimal complexity. All of the simulations were initially scaled based upon k/c from ice accretions obtained at the NASA Glenn Icing Research Tunnel (IRT). An alternative scaling method based upon the k/δ of the ice shape was also investigated for the low-fidelity simulations in some cases where scaling based on k/c was believed to be inappropriate. An investigation into the interaction between the boundary layer and the simulations was conducted using a combination of boundary-layer velocity measurements, fluorescent-oil flow visualization, and surface pressure measurements. This was done to investigate the scaling problem and understand the different aerodynamic effects of runback simulations scaled using the two methods.

Experimental Methods

Aerodynamic tests of simulated runback ice accretions were conducted in the Illinois 3 ft $\times$ 4 ft subsonic wind tunnel. The models tested had a chord of 18 in. and spanned the entire height of the test section. Two airfoils, the NACA 23012 and the NACA 3415, were selected to provide a range of clean-airfoil characteristics. Lee and Bragg [7] showed that the sensitivity of an airfoil to ridge-type ice simulations was dependant upon the chordwise loading of the airfoil. Hence, including two airfoils with different chordwise load distributions captured a range of penalties that could be expected from runback ice accretions. The NACA 23012 model had 68 chordwise pressure taps and 19 spanwise pressure taps. The NACA 3415 model had a trailing-edge flap that was set at 0 deg deflection for this test. The model had 78 chordwise pressure taps and 13 spanwise pressure taps.

A three-component force balance was used to measure the lift and pitching moments and the integrated turntable was used to set the angle of attack. A wake rake was located downstream of the model to collect total pressures in the wake, which were used to calculate the drag. The wake rake had 59 total pressure probes that were used to acquire the wake pressures. Both the wake and airfoil surface pressures were acquired with an electronically scanned pressure system. More information about the setup can be found in Lee [13].

Although surface pressure distributions were available, the lift coefficient and quarter-chord pitching-moment coefficient were derived only from the force balance. The pressure and balance data agreed very well for the clean-model configuration. However, larger differences were observed for the iced-model configurations because surface pressures could not be resolved accurately in the vicinity of simulated ice accretions. In addition, the runback ice simulations

Table 1 Estimated uncertainties for aerodynamic performance parameters

Aerodynamic quantity	Reference value	Absolute uncertainty	Relative uncertainty
α	5.00	±0.02	±0.40%
C_p	−0.712	±0.0037	±0.52%
C_l	0.295	±0.0016	±0.53%
C_m	−0.0791	±0.00039	±0.50%
C_d	0.0102	±0.00014	±1.40%

often covered a large chordwise area, eliminating multiple pressure taps and causing the integrated force and moment to be incorrect. Therefore, the data from the balance were more accurate. The drag coefficient was calculated from the wake pressures using standard momentum-deficit methods. All of these aerodynamic coefficients and the angle of attack were corrected for wall interference effects using the methods of Rae and Pope [14]. The experimental uncertainty in these coefficients was also estimated using the methods of Kline and McClintock [15] and Coleman and Steele [16] for 20:1 odds (Table 1). The uncertainties in α, C_l, and C_m were determined from the force-balance data and the remaining quantities (C_p, C_d) were determined from the pressure-based data. The values were determined by Lee [13] for freestream conditions of $Re = 1.8 \times 10^6$ and $M = 0.18$. All data reported in this paper correspond to this freestream condition.

In addition to aerodynamic performance measurements, two other tools were used to evaluate the effect of the two-dimensional ice simulations on the NACA 3415. Boundary-layer profile measurements were taken using a boundary-layer "rake" affixed to the surface of the model at the point where a profile measurement was desired. The rake consisted of an array of pitot tubes that simultaneously measured the total pressure at discrete points throughout the boundary-layer thickness and into the freestream. The static pressure, as measured by the nearest model-surface pressure tap, along with the total pressures from the rake were used to calculate the boundary-layer velocity profile. Fluorescent-oil flow visualization was also used to identify specific flow features and aid in the interpretation of airfoil surface pressure data.

Ice Accretion Simulation and Scaling

The scaled simulations were based on ice accretions collected during two tests at the NASA Glenn IRT. During those tests, a full-scale wing-section model equipped with a hot-air anti-icing system was used to generate runback ice accretions. Although the particular system used in this research was a hot-air system, the ice characteristics are typical of those observed for thermal deicing systems in general. The model had a span of 72 in., a root chord of 66.82 in., and a tip chord of 55.4 in. The airfoils used for the model were proprietary, but were of the type typically used for business jet-type aircraft. Three flight conditions were chosen because they represented critical operating points for the hot-air system of a typical aircraft configuration. The warm hold condition (Fig. 1) was critical to ice protection system (IPS) operation because it generated the highest water-catch rate based on Federal Aviation Regulation (FAR) Appendix C conditions [17]. The cold hold condition (Fig. 2) represented the largest temperature difference, based on Appendix C conditions, between the wing skin and the outside air. Finally, descent (Fig. 3) was critical for the IPS due to reduced engine power and, therefore, reduced bleed-air mass flow and temperature. Further details regarding the ice accretion testing can be found in Whalen et al. [1].

Because the aerodynamic investigations were limited to subscale, two-dimensional airfoil models, ice simulation and scaling were critical components of this work. Although the model used for the icing testing was three dimensional, that is, it was tapered, swept, and twisted, the magnitude of these features was small. Furthermore, the model was mounted floor to ceiling in the icing tunnel and there were no significant three-dimensional features observed in the ice accretion. The accretions, therefore, were used to guide the construction of representative runback-type ice simulations and should not be interpreted as particular to the airfoils used for aerodynamic performance testing. Simulations were constructed from observations of the castings as well as tracings of the ice profile at three spanwise locations and measurements of the accretion thickness. The basic approach to simulation construction was to use simple materials such as geometric substrates and roughness to simulate the ice as documented in the icing tests. These are referred to as "three-dimensional ice simulations." The castings did prove useful in this process as they provided the best documentation of the accretions. Follow-up simulations were also tested that were much simpler in nature, such as a square or rectangular cross section representing a ridge. These are referred to as "two-dimensional ice simulations." An advantage of these simpler simulations was that they could easily be varied parametrically in height and chordwise location. The combined aerodynamic results contributed to the understanding of the importance of simulation fidelity (i.e., how much of a difference does the extra geometry and roughness make?) as well as the sensitivity to height and chordwise location.

Geometrically Scaled Three-Dimensional Ice Simulations

The height of the simulations was not easy to characterize due to significant variations in height along the span of the accretion. For the simulations tested, the average of the accretion heights was taken and the height variation was simulated by the use of roughness elements. The overall height of the warm hold simulation on the suction surface (Fig. 4) was between 0.063 and 0.09 in., corresponding to a k/c

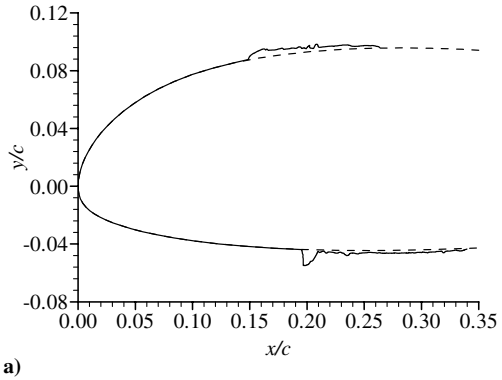

a)

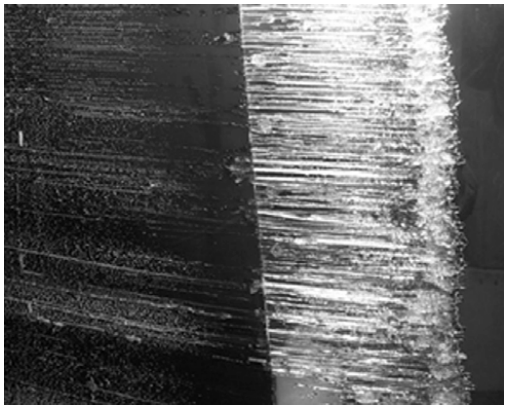

b)

Fig. 1 Tracing a) and photograph (flow is right to left) of suction surface b) for a 22.5 min exposure to warm hold conditions.

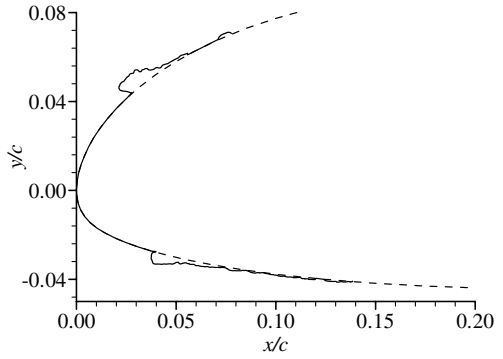

a)

b)

Fig. 2 Tracing a) and photograph (flow is right to left) of suction surface b) for a 22.5 min exposure to cold hold conditions.

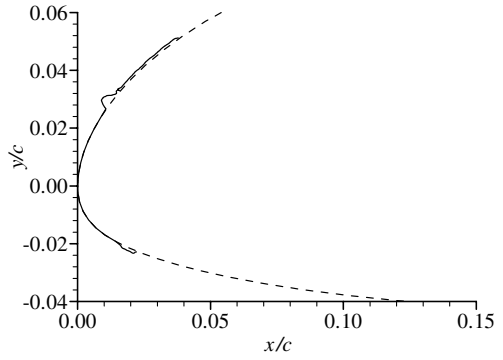

a)

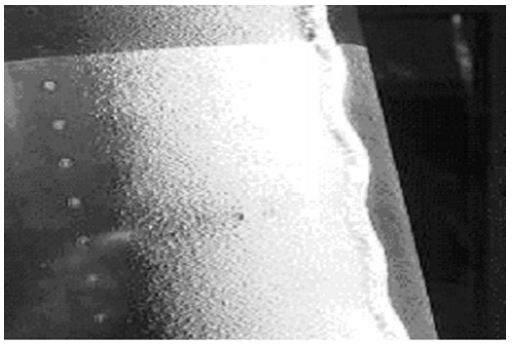

b)

Fig. 3 Tracing a) and photograph (flow is right to left) of suction surface b) for a 22.5 min exposure to descent conditions.

between 0.0035 and 0.005. The total height of the pressure-surface simulation varied between 0.15 and 0.25 in., equivalent to a k/c between 0.008 and 0.014, across the span. In the warm hold case the ice accretions began to form at approximately $x/c = 0.16$ on the suction surface and $x/c = 0.20$ on the pressure surface. More detailed descriptions of all of these simulations can be found in Whalen et al. [1].

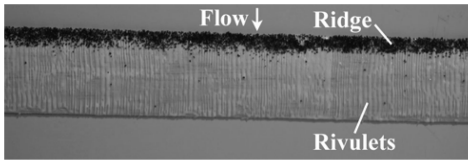

Fig. 4 Photograph of suction surface simulated warm hold ice simulation.

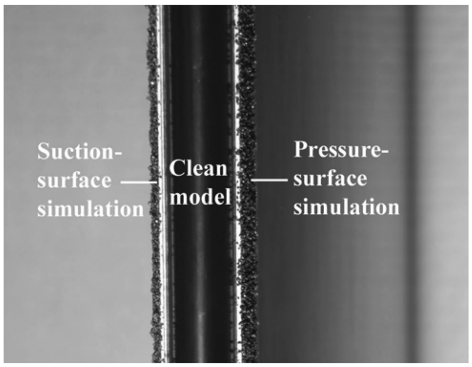

Fig. 5 Photograph of leading edge with installed simulated cold hold runback accretion.

The leading edge of the NACA 23012 with the cold hold simulations attached is shown in Fig. 5. The overall height of the suction-surface simulation with roughness was between 0.094 and 0.125 in., corresponding to a k/c between 0.005 and 0.007. The chordwise extent of the simulation was approximately 0.6 in. and the simulation spanned the entire model. A comparable simulation was constructed for the pressure surface. The thickness of the simulation with roughness was approximately 0.1 in., equivalent to a k/c of 0.006, and the chordwise extent was 0.625 in. The cold hold ice simulation was observed to begin at approximately $x/c = 0.015$ on the suction surface and $x/c = 0.035$ on the pressure surface.

The descent ice accretion was simulated with a simple ridge on the suction and pressure surface positioned at $x/c = 0.01$ and $x/c = 0.015$, respectively. The suction-surface ridge was a 0.063-in. ($k/c = 0.0035$) square section and the pressure-surface simulation consisted of 0.25 in., in the chordwise direction, of 36 grit roughness that is nominally 0.0232 in. ($k/c = 0.0013$) in diameter.

Geometrically and Boundary-Layer-Scaled Two-Dimensional Ice Simulations

In addition to the three-dimensional simulations, simplified two-dimensional simulations were also tested on the NACA 23012 and 3415 airfoils. The goal of the two-dimensional simulations was to represent the height of the runback ridge. Therefore, they had no roughness applied, had no spanwise variation and, unless otherwise stated in the discussion of the results, had a square cross section. The location of the two-dimensional simulation corresponded to the forward face of the runback ridge. The advantage of the two-dimensional simulations was that they allowed for easy parametric variation in height and chordwise location.

The two-dimensional simulations were scaled using both geometric and boundary-layer based methods. As in the three-dimensional simulations, the two-dimensional simulations were scaled according to the ratio of the chords of the ice accretion model and the aerodynamic model. Research by Lee and Bragg [4] and Broeren and Bragg [8] demonstrated that geometric scaling was an accurate method for simulating ice accretions. The simulations used in that research were over 20 times taller than the local boundary-layer thickness. In this study, the ice height was approximately

Table 2 Warm hold ice simulation scaling ($x/c = 0.16$, suction surface, δ calculated at $\alpha = 3$ deg)

	Geometric scaling			Boundary-layer scaling		
Airfoil	k, in.	k/c	k/δ	k, in.	k/c	k/δ
Full scale	0.232	0.0038	5.35	0.232	0.0038	5.35
NACA 23012	0.068	0.0038	2.44	0.149	0.0083	5.35
NACA 3415	0.068	0.0038	3.11	0.117	0.0065	5.35

Table 3 Cold hold ice simulation scaling ($x/c = 0.028$, suction surface, δ calculated at $\alpha = 3$ deg)

	Geometric scaling		
Airfoil	k, in.	k/c	k/δ
Full scale	0.412	0.0068	28.4
NACA 23012	0.122	0.0068	12.5
NACA 3415	0.122	0.0068	12.6

Table 4 Descent ice simulation scaling ($x/c = 0.01$, suction surface, δ calculated at $\alpha = -1$ deg)

	Geometric scaling		
Airfoil	k, in.	k/c	k/δ
Full scale	0.228	0.0037	41.38
NACA 23012	0.067	0.0037	15.55
NACA 3415	0.067	0.0037	15.33

10 times taller than the local boundary-layer thickness in the cold hold and descent cases. This made geometric scaling appropriate for those shapes. However, during the development of the test matrix it was noted that the heights of the warm hold simulations were approaching the thickness of the local boundary layer. Boundary-layer scaling used the ratio of the local boundary-layer thickness, on the clean airfoil at the ice simulation location, to the ice simulation height in order to scale the simulations. The authors are unaware of any studies where this has been demonstrated as a valid method for ice accretion simulation. However, the practice of using the Reynolds number Re_k, based on obstacle height and the velocity at the obstacle height in roughness studies has been documented extensively. As an example, a critical Re_k of approximately 600 for distributed three-dimensional roughness to induce transition of a laminar boundary layer is well known [18]. If, in fact, the relative height of the simulation to the boundary-layer thickness plays an important role in scaling these accretions, then the Reynolds number dependence may be larger than previously observed in iced-airfoil aerodynamics.

Boundary-layer scaling was carried out based upon the conditions at which the ice accretions were generated in the IRT. Namely, the Reynolds number, Mach number, and angle of attack were used as inputs to a boundary-layer code that calculated the boundary-layer thickness at the ice accretion locations. The code used integral boundary-layer parameters obtained from XFOIL [19] with the Falkner–Skan [20] solution for a laminar boundary layer and the Coles wake [21] solution for a turbulent boundary layer to calculate the local boundary-layer thickness.

Table 2 compares the heights of the warm hold ice simulations scaled geometrically and using the boundary-layer height. Scaling was carried out at $\alpha = 3$ deg, the angle of attack at which the ice was accreted. Because the boundary-layer thickness is a function of the angle of attack, k/δ decreases as the angle of attack is increased. As can be seen in the table, the boundary-layer-scaled ice simulations were over twice as tall as the geometrically scaled ice simulations. Tables 3 and 4 present the scaled-simulation heights for the cold hold and descent accretions, respectively. In those cases, boundary-layer scaling was not used because the simulations were significantly taller than the local, clean-model boundary-layer thickness even as the model approached stall. Therefore, geometric scaling based on chord length was expected to be appropriate, consistent with previous results for similar ridge-type shapes as discussed in the Introduction.

Results and Discussion

In this section the aerodynamic effects of each of the three types of runback ice simulations are considered. First, an investigation of the aerodynamic performance effects of the cold hold and descent simulations is presented. Second, the results for the warm hold simulations are examined. Finally, an alternative method of scaling the simulations, using the local boundary-layer thickness, was explored and flowfield investigations regarding the effects of the two-dimensional simulation were conducted. It is important to note that the aerodynamic performance penalties presented here pertain to the particular airfoils tested. However, the airfoils used were selected to provide a range of clean-airfoil characteristics. Hence, the results provide insight into the role of airfoil geometry in the effects of runback-type ice accretions and provide a range of aerodynamic performance effects due to runback-type ice accretions.

Cold Hold Ice Simulation

The performance penalties of geometrically scaled two-dimensional and three-dimensional cold hold ice simulations on the NACA 3415 are compared in Fig. 6. For the NACA 3415, the clean maximum-lift coefficient was 1.35, the stalling angle of attack was 13 deg, and the minimum drag coefficient was 0.0081. The two-dimensional ice simulation had a $k/c = 0.0069$ on the suction surface and a $k/c = 0.0052$ on the pressure surface. The suction-surface simulation was attached at $x/c = 0.028$ and the pressure-surface simulation was attached at $x/c = 0.035$. The three-dimensional ice simulation reduced the maximum-lift coefficient from 1.35 to 0.90, compared to 0.97 for the two-dimensional simulation, and caused a loss of 3 deg in stalling angle of attack compared to a loss of 2 deg in the two-dimensional simulation case. In both cases the stall exhibited classical thin airfoil behavior, making the stalling angle of attack and maximum-lift coefficient difficult to distinguish. Therefore, stall was identified from the break in the pitching moment. This behavior due to ridge formations has been observed in the past by Lee and Bragg [4]. The two-dimensional simulation results compared well with the work of Broeren et al. [9], which showed that a $k/c = 0.0055$ forward-facing quarter-round simulation at $x/c = 0.02$ reduced the maximum-lift coefficient of the NACA 3415 at $Re = 1.8 \times 10^6$ to approximately 1.05. Chordwise extent studies conducted at $x/c = 0.05$ with $k/c = 0.0069$ simulations indicated that chordwise extent did not significantly affect $C_{l\max}$ or α_{stall} [22]. Therefore, the greater chordwise extent of the three-dimensional simulation was likely not responsible for the greater penalties. The three-dimensional simulation did include a bull nose, that is a layer of the simulation extended forward of the attachment point of the base, feature to faithfully replicate the profile of the ice accretion. This feature, along with the roughness, may have acted to extract greater momentum from the boundary-layer flow causing a lower $C_{l\max}$ and α_{stall}.

Discrepancies between the two-dimensional and three-dimensional simulation results are not uncommon for ice simulations. Gurbacki and Bragg [23] found that for large horn shapes the maximum-lift penalty associated with the three-dimensional simulation was lower than that for the two-dimensional simulation. This was attributed to enhanced mixing, caused by the irregularities of the three-dimensional shape that shortened the separation bubble, relative to the two-dimensional case, following the simulation. However, Addy and Chung [24] tested a simulated horn shape on a NLF-0414 and found that the three-dimensional simulation caused greater lift penalties than the two-dimensional simulation. Later, Blumenthal et al. [25] conducted a parametric study of the effect of horn height by creating two-dimensional simulations based on ice tracings at multiple stations. They found that the variation in maximum-lift penalty due to the tracing location was consistent with

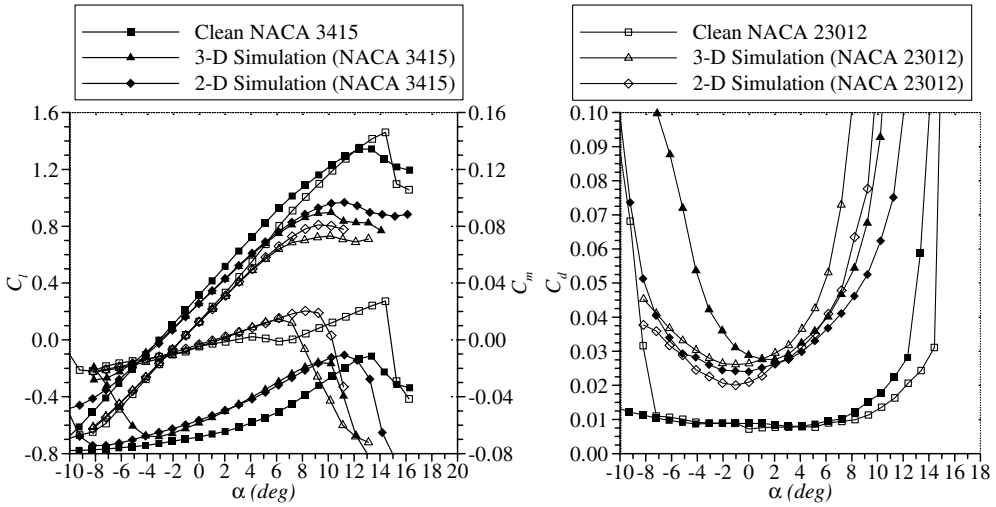

Fig. 6 Comparison of the effect of simulated two-dimensional and three-dimensional geometrically scaled cold hold ice simulations on the lift, drag, and pitching moment of the NACA 3415 and NACA 23012 ($Re = 1.8 \times 10^6$, $M = 0.18$).

the variations observed in previous studies, highlighting the importance of properly selecting the mean horn height. Drag penalty results were similar at moderate angles of attack, but were again greater in the three-dimensional case than in the two-dimensional simulation case for angles of attack leading up to stall. The minimum drag coefficient increased from the clean value of 0.0081 to 0.028 in the three-dimensional case and 0.026 in the two-dimensional case. Drag comparisons with other data were difficult to make in this case because both the pressure and suction-surface accretions were simulated and were particular to the cold hold accretion. The effects of the two-dimensional and three-dimensional simulations were relatively similar, especially compared to the warm hold case, indicating that simulation fidelity is not as great a concern for these types of runback simulations.

Performance penalties experienced by the NACA 23012 due to the same geometrically scaled two-dimensional and three-dimensional ice simulations that were tested on the NACA 3415 are also presented in Fig. 6. The maximum-lift coefficient was 1.46, the stalling angle of attack was 14 deg, and the minimum drag coefficient was 0.0078 for the clean NACA 23102. In contrast to the NACA 3415, the NACA 23012 exhibits an abrupt stall, indicating that it naturally stalls from the leading edge. McCullough and Gault [26] conducted extensive investigations into airfoil stall and found that leading-edge stall is typical of airfoils of moderate thickness such as the NACA 23012, while trailing-edge stall is typical for thicker airfoils such as the NACA 3415. The three-dimensional simulation reduced the $C_{l\max}$ from 1.46 to 0.73 versus 0.81 in the two-dimensional simulation case. Stalling angle of attack was reduced to 9 deg in the two-dimensional simulation case and 6 deg in the three-dimensional case. Lee and Bragg [4] found that for a $k/c = 0.0083$ forward-facing quarter-round at $x/c = 0.02$ the maximum-lift coefficient of the NACA 23012 at $Re = 1.8 \times 10^6$ was reduced to 0.76. This result compared nicely with the two-dimensional simulation result and indicates that the cold hold shape may have much in common, as far as aerodynamic penalty effects, with the quarter-round shape used by Lee and Bragg [4]. The greater penalties associated with the three-dimensional simulation may be attributed to the geometry (cross section) of the simulation and the added roughness. The minimum drag coefficient was increased from the clean value of 0.0078 to 0.026 in the three-dimensional case versus 0.020 in the two-dimensional simulation case. In general, the cold hold ice simulations had a greater effect on the NACA 23012 because of the higher pressure peak and steeper recovery that developed near the leading edge when compared to the NACA 3415. Here again, the effects of the two-dimensional and three-dimensional simulations on the performance of the NACA 23012 are quite similar. A summary of the performance effects of the two-dimensional and three-dimensional simulations on the two airfoils is presented in Table 5.

Morgan et al. [27] investigated the effects of frost-type ice shapes on a high-lift airfoil in the cruise configuration. Partial frost was simulated with roughness strips that had a k/c of 0.00045 extending from $x/c = 0.03$ to $x/c = 0.05$. Full frost was simulated with the same roughness strips extending to $x/c = 0.05$ on the upper and lower surfaces. They found that the maximum lift of the iced airfoil varied by less than 10% over a Reynolds number range from 3.0×10^6 to 12.0×10^6. Additionally, Broeren et al. [9] showed that the aerodynamic penalties of ridges with a k/c of 0.014 at $x/c = 0.02$, 0.10, and 0.20 were insensitive to Reynolds number, as described in the Introduction. The height ($k/c = 0.0069$) and chordwise location ($x/c = 0.015$) of the cold hold simulations lie within the range of those two studies. Therefore, Reynolds number is not expected to play a significant role in the performance effects of the cold hold simulations. Consequently, geometric scaling based on the chord length was appropriate and the results can be considered an accurate representation of the full-scale accretion.

Descent Ice Simulation

The aerodynamic effects of the simulated descent ice accretion (Fig. 3) are presented in Fig. 7. Only the results for the NACA 3415 are presented; results from the NACA 23012 were not available for comparison. However, aerodynamic penalty results for $k/c = 0.0035$ simulations from Calay et al. [5] on a NACA 0012 and Papadakis and Gile-Laflin [6] on a NACA 63_A213, both similar in thickness to the NACA 23012, were comparable to those observed for the NACA 3415. Here the ice accretion height was quite uniform across the span. There was no attempt to simulate the periodic

Table 5 Summary of the effects of geometrically scaled cold hold runback ice simulations on the NACA 3415 and NACA 23012 ($Re = 1.8 \times 10^6$ and $M = 0.18$)

	Clean			3-D simulation			2-D simulation		
Airfoil	$C_{l\max}$	α_{stall}	$C_{d\min}$	$C_{l\max}$	α_{stall}	$C_{d\min}$	$C_{l\max}$	α_{stall}	$C_{d\min}$
NACA 3415	1.35	13	0.0081	0.90	10	0.028	0.97	11	0.026
NACA 23012	1.46	14	0.0078	0.73	6	0.026	0.81	9	0.020

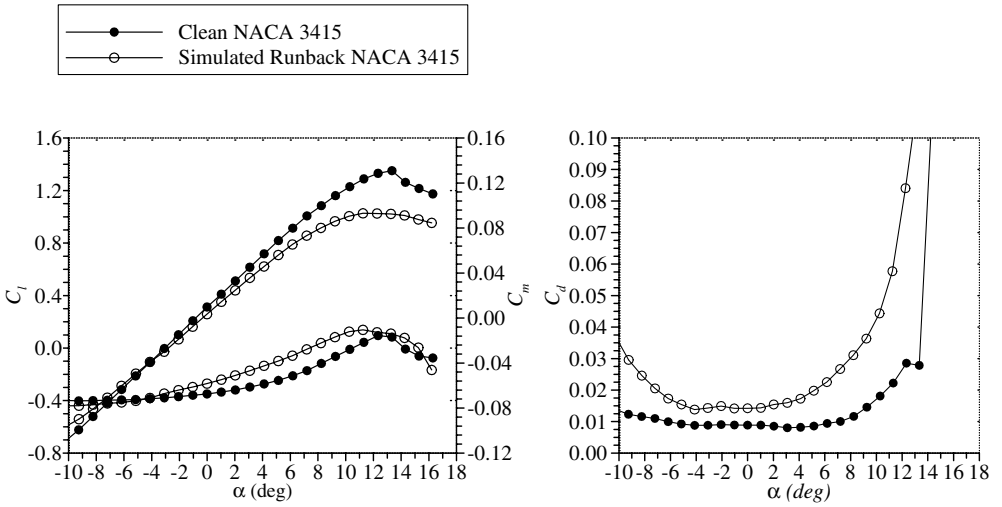

Fig. 7 Effect of a simulated three-dimensional descent ice simulation on the lift, drag, and pitching moment of the NACA 3415 ($Re = 1.8 \times 10^6$, $M = 0.18$).

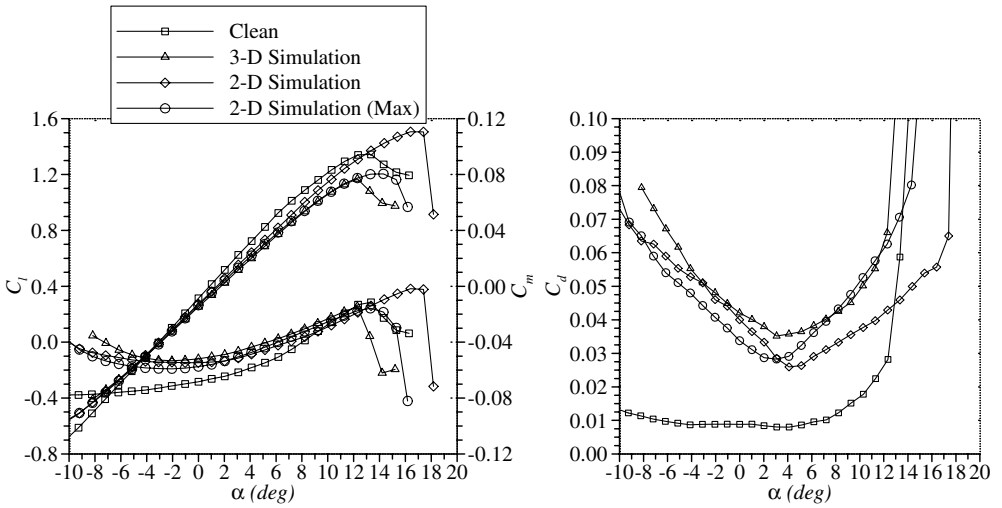

Fig. 8 Comparison of the effect of simulated three-dimensional and two-dimensional geometrically scaled warm hold ice simulations on the lift, drag, and pitching moment of the NACA 3415 ($Re = 1.8 \times 10^6$, $M = 0.18$).

variation in the chordwise position of the ridge. Instead, an average of the chordwise position of the accretion was chosen. The suction-surface simulation was located at $x/c = 0.01$ and had $k/c = 0.0035$. The pressure-surface simulation began at $x/c = 0.015$ and consisted of 36-grit roughness with a chordwise extent of 0.25 in. ($0.014c$) making the $k/c = 0.0013$. The minimum drag coefficient increased to approximately 0.014 in both the two-dimensional and three-dimensional cases. The maximum-lift coefficient of the NACA 3415 was reduced to 1.03 and the stalling angle of attack was reduced by 2 deg. The penalties associated with the descent simulation are summarized in Whalen et al. [1]. Icing exposure time for the descent case was 3.25 min versus 22.5 min for the warm and cold hold cases, making the effects of the descent simulation significant considering the short exposure time. Because the IPS supply air temperature and mass flow rate were reduced, the ridge grew rapidly and at a forward location, near $x/c = 0.01$, resulting in penalties similar to the warm and cold hold cases.

The simulation in this case was shorter and farther forward than in the cold hold case. Again, considering the location and height and in light of past investigations [7,8,27] Reynolds number was not expected to have a significant effect on the aerodynamic penalties of these simulations. The $C_{l\max}$ penalty in this case was greater than in the warm hold case, but the minimum drag was significantly less than in the warm or cold hold case. These facts are particularly significant when one considers that the descent may be leading up to a landing. In that case, the airplane may not return to a higher power setting that would allow the hot-air system to remove the accretion. The maximum-lift performance would be significantly degraded by a relatively short icing encounter creating a potentially dangerous flight condition.

Warm Hold Ice Simulation

The effects on the aerodynamic performance of the NACA 3415 with the geometrically scaled three-dimensional warm hold ice simulation are compared to those with the two-dimensional ice simulation in Fig. 8. In this study, both the suction- and pressure-surface accretions were simulated. The two-dimensional simulation had a $k/c = 0.0035$ on the suction surface and a $k/c = 0.012$ on the pressure surface. These dimensions were representative of the average of the ice thickness measurements made during the IRT test for the warm hold accretion. The three-dimensional simulation was shown to reduce the maximum-lift coefficient to 1.16 and lower the stalling angle of attack by 1 deg. It also increased the minimum drag coefficient to 0.035 from 0.0081. The two-dimensional simulation increased $C_{l\max}$ by 0.17 and increased $C_{d\min}$ to 0.026. It also increased α_{stall} by 4 deg. A two-dimensional simulation based on the maximum height measured from the full-scale accretion is also

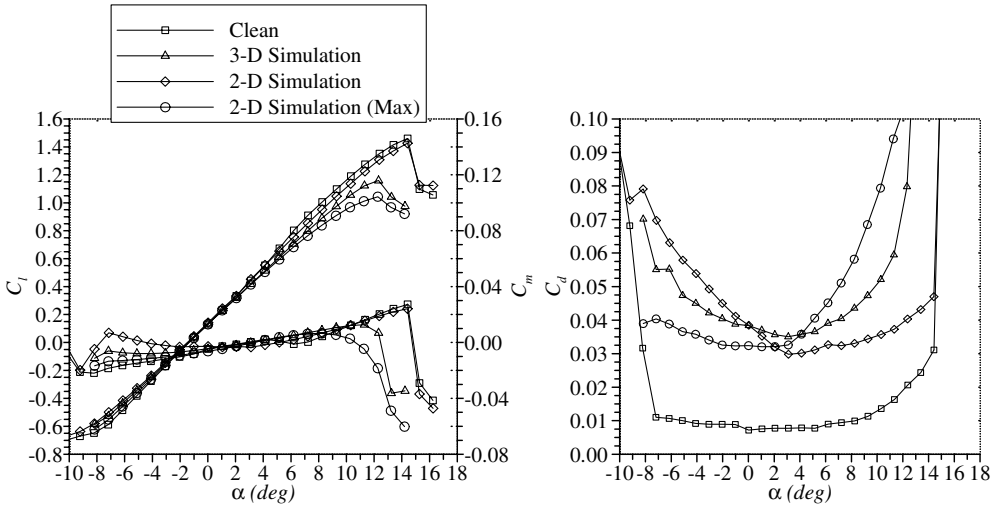

Fig. 9 Comparison of the effect of simulated three-dimensional and two-dimensional geometrically scaled warm hold ice simulations on the lift, drag, and pitching moment of the NACA 23012 ($Re = 1.8 \times 10^6$, $M = 0.18$).

included in Fig. 8. The ice simulation had a $k/c = 0.0052$. However, it was not representative of the overall ice simulation because it was based on an isolated feature of the accretion. It does demonstrate though, that there was a significant change in the effect of the ice simulation at this x/c location at k/c values between 0.0035, where there was a lift performance increase, and 0.005, where there was a lift performance penalty. The "2-D max" simulation decreased $C_{l\max}$ to 1.21 and increased $C_{d\min}$ to 0.028. The stalling angle of attack was unchanged by the simulation.

Performance effects of the same warm hold ice simulations tested on the NACA 3415 on the NACA 23012 are presented in Fig. 9. The three-dimensional simulation was found to reduce the maximum-lift coefficient to 1.16 and the stalling angle of attack to 12 deg. It also increased the minimum drag coefficient to 0.035. The geometrically scaled two-dimensional ice simulation had little effect on the maximum-lift performance of the NACA 23012, reducing $C_{l\max}$ to 1.42 from 1.46. However, the minimum drag increase to 0.030, from 0.0078, was similar to that experienced by NACA 3415 with the two-dimensional warm hold simulation attached. The two-dimensional simulation based on the maximum measured height again had a substantial effect on the performance, similar to that of the three-dimensional simulation, and appeared to alter the stalling character of the airfoil. The 2-D max simulation reduced the $C_{l\max}$ to 1.04 and increased $C_{d\min}$ to 0.032. The performance penalties of the warm hold simulations are summarized in Table 6. It is important to note that in all these cases (i.e., Figs. 8 and 9) the presence of the ice simulation reduced the lift-curve slope. It was only at high angle of attack that the geometrically scaled two-dimensional ice simulation was able to achieve any improvement in performance (for the NACA 3415 airfoil only).

Aerodynamic performance effects of simulated two-dimensional warm hold ice simulations on the performance of the NACA 3415 are shown in Fig. 10. The suction-surface ice simulations alone are presented to demonstrate the difference between the boundary layer and the geometrically scaled ice simulation. The goal of the two-dimensional ice simulations was to simulate the ice ridge rather than the entire extent of the ice simulation. Therefore, for example, in the warm hold case the two-dimensional simulation represents the ridge along with its height and location, but does not attempt to simulate

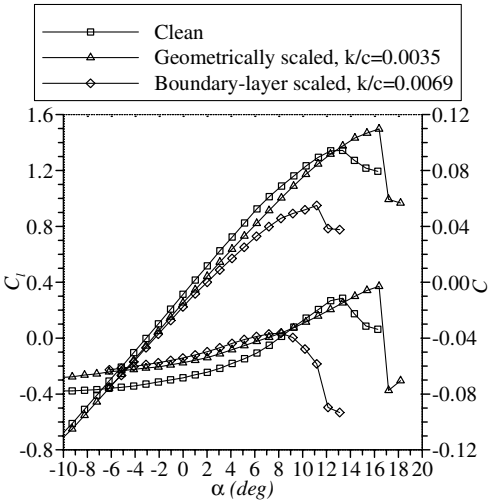

Fig. 10 Effect of a simulated two-dimensional warm hold ice simulation (suction-surface only) on the lift, drag, and pitching moment of the NACA 3415 ($Re = 1.8 \times 10^6$, $M = 0.18$).

the rivulets and other downstream structures. In the geometrically scaled case, a $k/c = 0.0035$ square shape was positioned at $x/c = 0.16$ to simulate the warm hold ice accretion. Interestingly, α_{stall} increased by 4 deg and the $C_{l\max}$ increased to 1.52. This is the effect that motivated the investigation of Reynolds number effects on the subscale model boundary-layer behavior as a factor in the performance effects of these ice simulations. Note that the character of the stall changed as a result of the geometrically scaled ice simulation. It became much more abrupt in both the loss of lift and the change in the pitching moment. This indicated that the airfoil was stalling from the leading edge rather than from the trailing edge, as it did in the clean case. The boundary-layer-scaled ice simulation had a $k/c = 0.0069$ and was positioned at $x/c = 0.16$. It reduced $C_{l\max}$ to 0.95 and caused a 2-deg reduction in stalling angle of attack. For the boundary-layer-scaled ice simulation, the stall character appeared to

Table 6 Summary of the effects of geometrically scaled warm hold runback ice simulations on the NACA 3415 and NACA 23012 ($Re = 1.8 \times 10^6$ and $M = 0.18$)

	Clean			3-D simulation			2-D simulation		
Airfoil	$C_{l\max}$	α_{stall}	$C_{d\min}$	$C_{l\max}$	α_{stall}	$C_{d\min}$	$C_{l\max}$	α_{stall}	$C_{d\min}$
NACA 3415	1.35	13	0.0081	1.16	12	0.035	1.52	17	0.026
NACA 23012	1.46	14	0.0078	1.16	12	0.035	1.42	14	0.030

Table 7 Summary of the effects of three-dimensional runback ice simulations on the NACA 3415 and NACA 23012 ($Re = 1.8 \times 10^6$, $M = 0.18$)

	Clean			Cold hold			Descent			Warm hold		
Airfoil	$C_{l\max}$	α_{stall}	$C_{d\min}$	$C_{l\max}$	α_{stall}	$C_{d\min}$	$C_{l\max}$	α_{stall}	$C_{d\min}$	$C_{l\max}$	α_{stall}	$C_{d\min}$
NACA 3415	1.35	13	0.0081	0.90	10	0.028	1.03	11	0.014	1.16	12	0.035
NACA 23012	1.46	14	0.0078	0.73	6	0.026	N/A	N/A	N/A	1.16	12	0.035

be more like that of the clean airfoil, that is, trailing-edge type. The effects of geometrically scaled, three-dimensional simulations of warm hold, cold hold, and descent runback simulations at $Re = 1.8 \times 10^6$ and $M = 0.18$ are summarized in Table 7.

Lift Enhancement Caused by Ridge-Type Ice Simulations

Another motivation for exploring the boundary-layer scaling of these ice simulations was to investigate the phenomenon by which α_{stall} and $C_{l\max}$ are increased by the presence of the geometrically scaled warm hold ice simulations. This investigation was conducted using the NACA 3415 model because the effect was most prominent for that airfoil. As will be discussed, because the clean NACA 23012 stalls from the leading edge, it does not benefit to the same degree from the apparent boundary-layer modification caused by the geometrically scaled ($k/c = 0.0035$) simulation as does the NACA 3415, which stalls from the trailing edge. This suggests that the mechanism by which the performance is typically degraded, ostensibly the premature separation of the boundary layer on the aft part of the model, was avoided. The fact that the stall type remains sharp in the two-dimensional case, but becomes more gradual with the 2-D max simulation indicates that this was indeed the case (i.e., the model stalled from the leading edge with the two-dimensional shape, but had a significant trailing-edge stall component in the 2-D max case).

Fluorescent-oil flow visualization was used to visualize the surface flowfield structures associated with the geometrically and boundary-layer-scaled simulations. A brief description of the oil flow visualization technique will aid in interpreting the photographs. Fluorescent-oil flow visualization is used to indicate the magnitude of the surface shear, which is used to infer the state of the boundary layer at a given location. Oil patterns can also provide information regarding the flow direction along the surface of the model. To begin the process, oil is sprayed in a fine mist onto the surface of the model creating a stippled pattern of oil droplets likened to the appearance of an orange peel. The model is then run at the selected angle of attack and Reynolds number for a predetermined length of time that allows the desired mean structures to establish a pattern in the oil. Illuminating the fluorescent oil with ultraviolet light facilitates the visualization of the flow patterns that is recorded with photographs like the ones presented here. In regions of attached flow with sufficient surface shear oil is drawn out into lines along the mean flow direction. The more oil that is wiped from the surface by the flow the higher the local shear. In regions of very low surface shear, such as at reattachment or in areas of separated flow, the oil retains its original stippled appearance. A line of oil accumulates in regions where the flow meets traveling in opposite directions or at points where the oil flows into an obstacle.

Results from fluorescent-oil flow visualization for the NACA 3415 at $\alpha = 16$ deg with the geometrically scaled simulation ($k/c = 0.0035$) located at $x/c = 0.16$ are presented in Fig. 11. A strip of tape was affixed to the model at the top and bottom of the frame to indicate the chordwise position in percent of chord. Also, a label in the lower-left corner listed the run conditions. The oil accumulation lines forward and aft of the simulation are the result of the seam of the tape used to attach the simulation to the model. Sixteen degrees angle of attack corresponded to $C_{l\max}$ for that case (Fig. 10). In Fig. 11 transition was apparent near the leading edge, followed by a faint stippled zone at approximately $x/c = 0.22$ where the flow reattached after separating from the ice simulation. Transition occurred via a small laminar separation bubble indicated by the oil accumulation line in the transition region. Flow transition was evidenced by the nearly complete wiping of oil from the surface in the region following the oil accumulation line. This was a result of the high surface shear associated with the turbulent boundary layer. The transition feature is described further in the boundary-layer-scaled simulation case where it is more clearly visible. Trailing-edge separation then occurred between $x/c = 0.60$ and $x/c = 0.65$. Stall in this case resulted from the collapse of the leading-edge pressure peak that was developed because of the separation bubble just aft of the ice simulation. This will be made more apparent with a discussion of the static pressure distribution associated with this simulation.

In the case of the boundary-layer-scaled ice simulation ($k/c = 0.0069$) the most striking difference from the geometrically scaled case was the much longer separation bubble following the simulation. In addition, results for several angles of attack showed that the reattachment zone moved aft rapidly with angle of attack. An example of a fluorescent-oil flow visualization result at $\alpha = 8$ deg for the NACA 3415 with the boundary-layer-scaled simulation is shown in Fig. 12. The corresponding performance data were presented in Fig. 10. Transition, via a small laminar separation bubble, was clearly visible near $x/c = 0.09$. The oil accumulation line indicated a discontinuity in the surface shear and the stippled appearance aft of it indicated a region of low surface shear, both consistent with a separation bubble. Breaks in the oil accumulation line were the result of surface contaminants or imperfections that caused the flow to transition locally ahead of the bubble. In Fig. 12 the reattachment zone following separation from the ice simulation was clearly visible near $x/c = 0.40$ and trailing-edge separation was indicated to occur near $x/c = 0.75$. At $\alpha = 9$ deg (not shown), there appeared to be some reverse flow in the region between the ice simulation and approximately $x/c = 0.40$, however, there was no evidence of attached flow following the line that divided the reverse flow from the flow aft of it. This was consistent with the slope change in the lift-curve slope and "break" in the pitching moment at that angle of attack. It also demonstrated that the bubble was no longer closed past $\alpha = 9$ deg and the flow was separating from the ice simulation and not reattaching to the airfoil. Results at several angles of attack suggested that separation progressed forward rapidly from

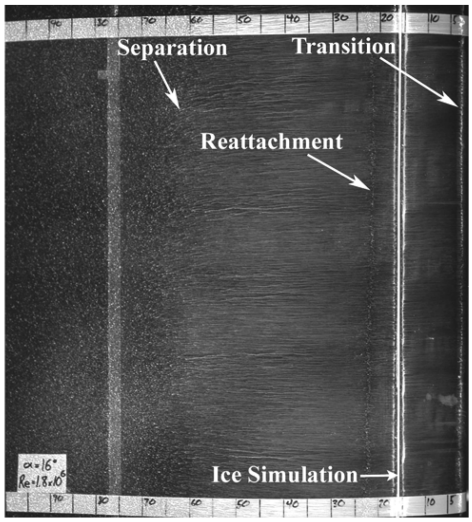

Fig. 11 Fluorescent-oil flow visualization at $\alpha = 16$ deg for the NACA 3415 with the geometrically scaled ($k/c = 0.0035$) two-dimensional warm hold ice simulation. ($Re = 1.8 \times 10^6$, $M = 0.18$).

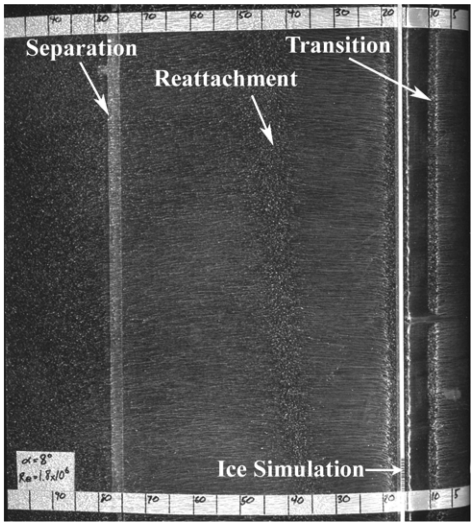

Fig. 12 Fluorescent-oil flow visualization at $\alpha = 8$ deg for the NACA 3415 with the boundary-layer-scaled ($k/c = 0.0069$) two-dimensional warm hold ice simulation attached. ($Re = 1.8 \times 10^6$, $M = 0.18$).

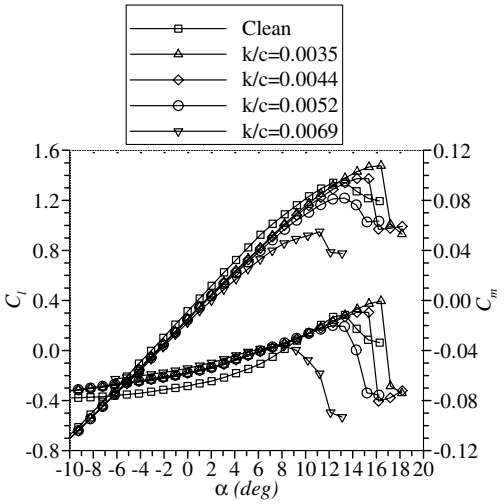

Fig. 14 Effect of ice simulation height at $x/c = 0.16$ on the NACA 3415 ($Re = 1.8 \times 10^6$, $M = 0.18$).

the trailing edge to meet the separation bubble growing rearward to cause stall.

The results of the flow visualization are summarized in Fig. 13. For the boundary-layer-scaled case, flow visualization showed that trailing-edge separation progressed rapidly forward as angle of attack increased and that the separation bubble was much larger than in the geometrically scaled case. The separation bubble in the geometrically scaled case remained approximately 5 to 7% of the chord up to stall (Fig. 13a) and trailing-edge separation progressed only to approximately $x/c = 0.65$ at stall. In the boundary-layer-scaled case, the separation bubble was 30 to 40% of the chord before stall (Fig. 13b). In addition, the flow appeared to be separated directly from the ice simulation at angles of attack greater than 8 deg.

The effect of ice simulation height at $x/c = 0.16$ on the performance of the NACA 3415 is illustrated in Fig. 14. Two ice simulation heights, $k/c = 0.0044$ and $k/c = 0.0052$, were tested in addition to the two-dimensional geometrically and boundary-layer-scaled warm hold ice simulation, which were $k/c = 0.0035$ and $k/c = 0.0069$, respectively. Stall was delayed by the $k/c = 0.0035$, as discussed earlier, and $k/c = 0.0044$ ice simulations. However, the $k/c = 0.0052$ ice simulation reduced the $C_{l\max}$ of the airfoil and maintained the same α_{stall} as the clean airfoil. At some height between $k/c = 0.0044$ and $k/c = 0.0052$ the performance effect of the ridge clearly changed from improving to degrading the high angle-of-attack performance of the airfoil.

A comparison of k/δ as a function of $C_l/C_{l\max}$ for the ice simulations tested in the present study to those tested by Calay [5] and Papadakis [6] is presented in Fig. 15. The figure plots the ratio of the simulation height to the local boundary-layer thickness on the clean model as a function of the ratio of the clean-model C_l to the clean-model $C_{l\max}$. The Reynolds number for these cases ranged from 1.25×10^6 to 2.0×10^6. Additionally, the Calay and Papadakis simulations were located at $x/c = 0.15$ versus $x/c = 0.16$ for the present study. The conclusion from Fig. 15 was that ice simulations that were observed to cause a performance increase had a k/δ near one as the airfoil approached $C_{l\max}$. In contrast to those ice simulations, the boundary-layer-scaled ice simulation, with a $k/c = 0.0069$, had a k/δ greater than 2 as the airfoil approached stall. This demonstrated that the relative height of the ice simulation to the boundary layer played a significant role in the phenomenon. It also showed that simple geometric scaling of runback ice accretions may not be sufficient to accurately describe their aerodynamic effects.

Boundary-layer profile measurements for the geometrically scaled ($k/c = 0.0035$) two-dimensional ice simulation at $\alpha = 8$ deg are presented in Figs. 16 and 17 and show the same measurements for the boundary-layer-scaled ($k/c = 0.0069$) two-dimensional ice simulation. In those plots the height normal to the surface of the model (n)

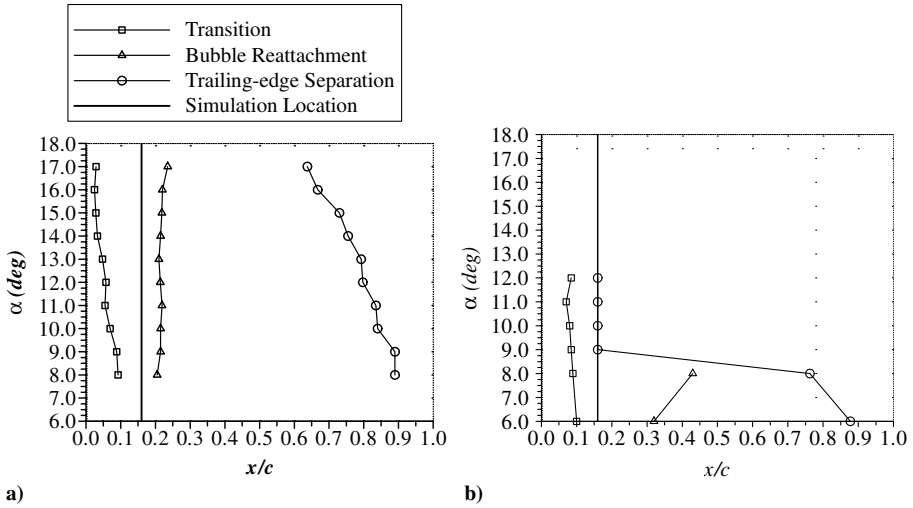

Fig. 13 Fluorescent-oil flow visualization analysis with a) the geometrically scaled ($k/c = 0.0035$) and b) the boundary-layer-scaled ($k/c = 0.0069$) warm hold ice simulation at $x/c = 0.16$ (NACA 3415, $Re = 1.8 \times 10^6$, $M = 0.18$).

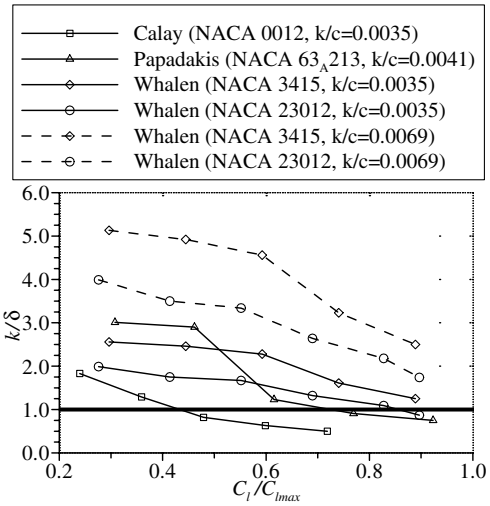

Fig. 15 Comparison of k/δ for various ice simulations at $x/c = 0.15$ (Calay [5] and Papadakis [6]) and 0.16 (Whalen).

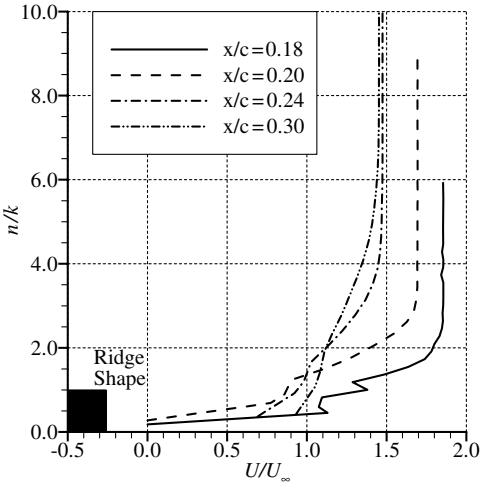

Fig. 16 Boundary-layer profile measurements at $x/c = 0.18$, 0.20, 0.24, and 0.30 at $\alpha = 8$ deg for the geometrically scaled ($k/c = 0.0035$) two-dimensional warm hold ice simulation (NACA 3415, $Re = 1.8 \times 10^6$, $M = 0.18$).

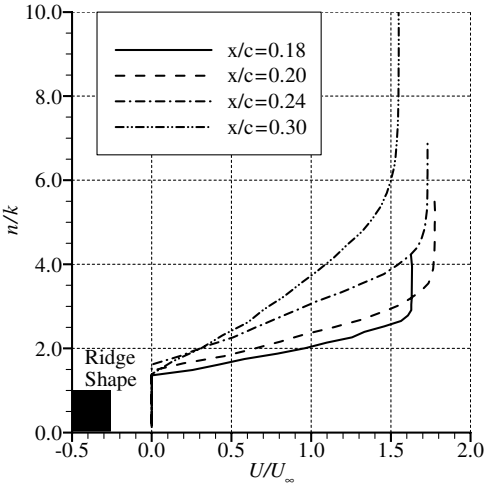

Fig. 17 Boundary-layer profiles measurements at $x/c = 0.18$, 0.20, 0.24, and 0.30 at $\alpha = 8$ deg for the boundary-layer-scaled ($k/c = 0.0069$) two-dimensional warm hold ice simulation (NACA 3415, $Re = 1.8 \times 10^6$, $M = 0.18$).

was normalized by the simulation thickness (k) and plotted against the ratio of the local velocity to the freestream velocity. The boundary-layer flow was quite different between the two ice simulations. Pitot tubes were used to collect the pressure data from which local flow velocity was calculated. Because pitot tubes do not read correctly in areas of reverse flow these areas are indicated as zero velocity in the figures. In the case of the geometrically scaled ice simulation, the only zero velocity reported was at the lowest pitot tube positioned at approximately $n/k = 0.20$. At $n/k = 0.47$ and 1.0 there were sharp increases in the local velocity. Subsequent measurements at $x/c = 0.20$, 0.24, and 0.30 showed that these sharp changes in the velocity in the boundary layer were not present by $x/c = 0.20$. However, some remnant of them persisted, manifested as a slope change in the profile that remained within the boundary layer to $x/c = 0.30$, the farthest aft station where measurements were taken. At $x/c = 0.20$ the slope change extended from $n/k = 0.70$ to 1.3 and at $x/c = 0.30$ the slope change persisted from approximately 0.44 to 2.2. It was difficult to ascertain reattachment from these data, but flow visualization showed that the separation bubble reattached near $x/c = 0.20$. The boundary-layer profiles for the boundary-layer-scaled ice simulation (Fig. 17) showed a large region of reverse flow that reached a maximum thickness of $n/k = 1.6$ near $x/c = 0.24$ and decreased in height by $x/c = 0.30$. Flow visualization showed that the separation bubble reattached between $x/c = 0.35$ and 0.42. The wide reattachment zone indicated that the separation-bubble reattachment was quite unsteady. Clearly, the geometrically scaled ice simulation was able to modify the boundary-layer flow while only creating a small, stable, separation bubble while the boundary-layer-scaled ice simulation generated a large separation bubble. This modification allowed the boundary layer to remain attached at angles of attack greater than the clean stalling angle of attack by entraining higher momentum fluid from the outer flow and delaying the advancement of the trailing-edge separation. The large separation bubble generated by the boundary-layer-scaled ice simulation removed momentum from the boundary layer and hastened the advancement of the trailing-edge separation, causing the airfoil to stall earlier.

Analysis of the pressure distributions on the model as a result of these ice simulations indicated a related effect to the fluid entrainment described above. The pressure profiles for the NACA 3415 are shown in Fig. 18 for the geometrically scaled warm hold ice simulation ($k/c = 0.0035$) installed at $x/c = 0.16$. Because of the presence of the simulation, the suction peak at the leading edge was allowed to grow to over 30% greater than the clean suction peak. Also, the acceleration of the flow over the ice simulation generated an abrupt decrease in C_p. The subsequent rapid increase in C_p and return to the clean C_p indicated the presence of a short separation bubble following the ice simulation. At angles of attack greater than the clean stalling angle of attack the delay in trailing-edge separation caused by the ice simulation allowed the circulation of the airfoil to continue to increase, driving the stagnation point farther aft on the pressure surface and resulting in greater flow acceleration near the leading edge. The recovery that followed the second pressure peak was gentle in comparison to that of the leading-edge peak and decreased in slope with angle of attack. This, in a sense, insulated the flow aft of the simulation from the steep adverse pressure gradient near the leading edge. Maximum lift was increased over the clean-model value by the higher suction peak and the added low pressure in the vicinity of the ice. Ultimately, the boundary layer separated from the ridge and failed to reattach. Oil flow visualization showed that the flow was still attached up to the ridge after stall was indicated by the performance data. It is important to note that up to $\alpha = 13$ deg the pressure peak was lower in magnitude, for the same angle of attack, with the ice simulation installed than it was in the clean case. A reduction in the lift-curve slope at low angle of attack was observed for this simulation, which was consistent with the reduction in the leading-edge suction peak at those angles of attack.

In the case of the boundary-layer-scaled warm hold ice simulation ($k/c = 0.0069$) the C_p preceding the ice simulation was much greater than seen with the $k/c = 0.0035$ ice simulation,

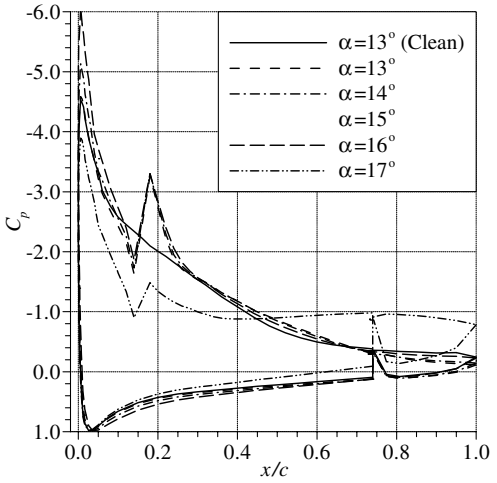

Fig. 18 NACA 3415 pressure profiles near maximum lift with the geometrically scaled ($k/c = 0.0035$) ice simulation installed at $x/c = 0.16$ ($Re = 1.8 \times 10^6$, $M = 0.18$).

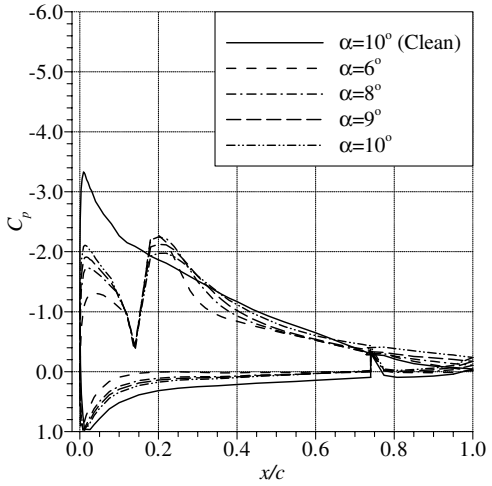

Fig. 19 NACA 3415 pressure profiles near maximum lift with the boundary-layer-scaled ($k/c = 0.0069$) ice simulation installed at $x/c = 0.16$ ($Re = 1.8 \times 10^6$, $M = 0.18$).

approximately −0.4 versus −1.8 (Fig. 19). Trailing-edge separation appeared to be extensive; this was confirmed by flow visualization (Fig. 13). The airfoil was unable to generate a substantial leading-edge suction peak due to the trailing-edge separation and flow retardation ahead of the ice simulation. In fact, the secondary peak, caused by flow acceleration around the ice simulation, was greater in magnitude than the leading-edge suction peak. In addition, the low pressure region caused by the ice simulation was greater in chordwise extent, indicating the greater extent of the separation bubble in that case. The secondary peak accounted for the fact that there was not a more significant penalty in lift at low angles of attack when compared to the effect of the $k/c = 0.0035$ ice simulation (Fig. 10).

Conclusions

The objectives of this study were to measure the aerodynamic performance penalties of selected runback ice simulations and to investigate methods for the simulation and scaling of these shapes. Ice simulations were based on accretions obtained at the NASA IRT from the testing of a wing section equipped with a hot-air anti-icing system. Aerodynamic performance testing was carried out at the Illinois 3 ft × 4 ft subsonic wind tunnel using two airfoil models, the NACA 23012 and the NACA 3415. The ice simulations were scaled based on k/c and k/δ and were simulated at two levels of fidelity, resulting in so-called two-dimensional and three-dimensional simulations. In addition to aerodynamic performance testing, fluorescent-oil flow visualization, boundary-layer velocity measurements, and surface pressure distributions were used to examine the interaction between the simulations and the model flowfield.

The most significant aerodynamic performance penalties were associated with the cold hold simulations where the maximum-lift coefficient of the NACA 23012 was reduced from 1.43 in the clean case to 0.73 and the stalling angle of attack was reduced to 6 deg from 14. In general, the NACA 23012 suffered worse performance degradations due to the ice simulations than did the NACA 3415. Because of the forward loading of the NACA 23012 it is more sensitive to ice accretions than the NACA 3415, which is more aft loaded. Comparisons of the two-dimensional and three-dimensional penalties of cold hold simulations indicated that simulation fidelity was not critical to capturing aerodynamic performance penalties of the cold hold simulations. The penalties associated with the descent simulations were significant when one considers the relatively short icing exposure time, 3.5 versus 22.5 min, compared to the warm and cold hold icing encounters. Reductions in maximum lift and stalling angle of attack were greater for the descent case than for the warm hold case. The question of the importance of simulation fidelity for descent accretions is not fully answered. The uniformity of height and very fine roughness associated with the descent shapes made the two-dimensional and three-dimensional simulations indistinguishable for this test and so only a three-dimensional simulation was tested. However, the effect of the periodic variation of the chordwise position of the ridge along the span is not known at this time. Effects of cold hold and descent simulations were, however, comparable to the results of previous tests of ridge-type accretions. Furthermore, the height and chordwise position of the simulations were consistent with those for shapes that did not exhibit significant variations in their effects due to Reynolds number. Therefore, geometric scaling of these types of ice shapes is expected to result in performance penalties that are representative of full scale.

Warm hold simulations did not exhibit good agreement between the two-dimensional and three-dimensional simulations. The performance effects were shown to be very sensitive to simulation height and fidelity. In fact, the three-dimensional simulation had a detrimental effect on the performance of both airfoils, while the two-dimensional simulation enhanced (NACA 3415) or had little effect on (NACA 23012) the maximum-lift coefficient and stalling angle of attack. Compared to the cold hold and descent simulations the warm hold simulations were quite far aft on the airfoils and short relative to the boundary layer. Unlike the cold hold and descent simulations Reynolds number considerations and effects may be important in characterizing the aerodynamic penalties of these ice simulations. The boundary-layer scaling method employed here was an attempt to account for those effects and ascertain the potential aerodynamic penalties of the warm hold accretions. The potential magnitude of this dependence was demonstrated by the comparison of the geometrically and boundary-layer-scaled warm hold simulations. The geometrically scaled warm hold simulation *increased* the maximum-lift coefficient by 0.17, while the boundary-layer-scaled simulation *decreased* it by 0.40. Because of this, full-scale aerodynamic penalty results for cast runback ice accretions are especially important to provide a baseline for the evaluation of scaled warm hold simulations because of the small k/δ and aft x/c locations associated with those accretions.

Investigations into the flowfields resulting from the geometrically and boundary-layer-scaled two-dimensional simulations revealed significant differences between the two. The geometrically scaled simulation generated a small, stable separation bubble aft of the simulation and caused an increase in the maximum-lift coefficient and stalling angle of attack of the model. It accomplished this by delaying the advancement of the trailing-edge separation associated with the stall of the clean model. Conversely, the boundary-layer-scaled simulation generated a large, fast-growing separation bubble aft of the simulation and caused significant losses in both maximum-lift coefficient and stalling angle of attack.

Acknowledgments

The authors would like to recognize several people who made this research program possible. The authors at the University of Illinois were supported, in part, by the Federal Aviation Administration (FAA) under grant DTFA 96-G-023. We would also like to thank Jim Riley and Gene Hill, from the FAA. We would like to acknowledge the Icing Branch at NASA John H. Glenn Research Center at Lewis Field for supporting the ice accretion testing. Specifically, we would like to thank Gene Addy, Tom Bond, Sam Lee, and the staff at the NASA Glenn Icing Research Tunnel (IRT).

References

[1] Whalen, E. A., Broeren, A. P., Bragg, M. B., and Lee, S., "Characteristics of Runback Ice Accretions on Airfoils and Their Aerodynamic Effects," AIAA Paper 2005-1065, Jan. 2005.

[2] Gray, V. H., and von Glahn, U. H., "Effect of Ice and Frost Formations on Drag of NACA 65B1B-212 Airfoil for Various Modes of Thermal Ice Protection," NACA TN-2962, June 1953.

[3] Jacobs, E. N., "Airfoil Characteristics as Affected by Protuberances," NACA, Rept. 446, 1932.

[4] Lee, S., and Bragg, M. B., "Experimental Investigation of Simulated Large-Droplet Ice Shapes on Airfoil Aerodynamics," *Journal of Aircraft*, Vol. 36, No. 5, Sept.–Oct. 1999, pp. 844–850.

[5] Calay, R. K., Holdo, A. E., and Mayman, P., "Experimental Simulation of Runback Ice," *Journal of Aircraft*, Vol. 34, No. 2, March–April 1997, pp. 206–212.

[6] Papadakis, M., and Gile-Laflin, B. E., "Aerodynamic Performance of a Tail Section with Simulated Ice Shapes and Roughness," AIAA Paper 2001-0539, Jan. 2001.

[7] Lee, S., and Bragg, M. B., "Investigation of Factors Affecting Iced-Airfoil Aerodynamics," *Journal of Aircraft*, Vol. 40, No. 3, May–June 2003, pp. 499–508.

[8] Broeren, A. P., and Bragg, M. B., "Effect of Airfoil Geometry on Performance with Simulated Intercycle Ice Accretions," *Journal of Aircraft*, Vol. 42, No. 1, Jan.–Feb. 2005, pp. 121–130.

[9] Broeren, A. P., Lee, S., LaMarre, C. M., and Bragg, M. B., "Effect of Airfoil Geometry on Performance with Simulated Ice Accretions Volume 1: Experimental Investigation," Federal Aviation Administration, Washington, D.C., Office of Aviation Research DOT/FAA/AR-03/64, Aug. 2003.

[10] Schofield, W. H., and Logan, E., "Turbulent Shear Flow over Surface Mounted Obstacles," *Transactions of the ASME Journal of Fluids Engineering*, Vol. 112, Dec. 1990, pp. 376–385.

[11] Sullerey, R. K., Mishra, S., and Pradeep, A. M., "Application of Boundary Layer Fences and Vortex Generators in Improving Performance of S-Duct Diffusers," *Transactions of the ASME Journal of Fluids Engineering*, Vol. 124, No. 1, March 2002, pp. 136–142.

[12] Lin, J. C., "Review of Research on Low-profile Vortex Generators to Control Boundary-Layer Separation," *Progress in Aerospace Sciences*, Vol. 38, Nos. 4–5, May/July 2002, pp. 389–420. doi:10.1016/S0376-0421(02)00010-6

[13] Lee, S., "Effect of Supercooled Large Droplet Icing on Airfoil Aerodynamics," Ph.D. Dissertation, Department of Aeronautical and Astronautical Engineering, Univ. of Illinois, Urbana, IL, 2001.

[14] Rae, W. H., and Pope, A., *Low-Speed Wind Tunnel Testing*, 2nd ed., Wiley, New York, 1984, pp. 349–362.

[15] Kline, S. J., and McClintock, F. A., "Describing Uncertainties in Single-Sample Experiments," *Mechanical Engineering*, Vol. 75, No. 1, Jan. 1953, pp. 3–8.

[16] Coleman, H. W., and Steele, W. G., *Experimentation and Uncertainty Analysis for Engineers*, Wiley, New York, 1989, pp. 40–118.

[17] Federal Aviation Administration Pt. 25 (FAR 25), "Airworthiness Standards: Transport Category Airplanes, Appendix C," Washington, D.C., Department of Transportation, Federal Aviation Administration, 1974.

[18] Braslow, A. L., and Knox, E. C., "Simplified Methods for Determination of Critical Height of Distributed Roughness Particles for Boundary-Layer Transition at Mach Numbers from 0 to 5," NACA TN-4363, Sept. 1958.

[19] Drela, M., XFOIL Subsonic Airfoil Development System, http://raphael.mit.edu/xfoil/.

[20] White, F. M., *Viscous Fluid Flow*, 2nd ed., McGraw–Hill, New York, 1991, pp. 242–247.

[21] Coles, D., "The Law of the Wake in the Turbulent Boundary-Layer," *Journal of Fluid Mechanics*, Vol. 1, Pt. 2, July 1956, pp. 191–226. doi:10.1017/S0022112056000135

[22] Whalen, E. A., Broeren, A. P., and Bragg, M. B., "Reynolds Number Considerations for Aerodynamic Testing of Simulated Runback Ice Accretions," AIAA Paper 2006-0260, Jan. 2006.

[23] Gurbacki, H. M., and Bragg, M. B., "Unsteady Aerodynamic Measurements on an Iced Airfoil," AIAA Paper 2002-0241, Jan. 2002.

[24] Addy, H. E., and Chung, J. J., "A Wind Tunnel Study of Icing Effects on a Natural Laminar Flow Airfoil," AIAA Paper 2000-0095, Jan. 2000.

[25] Blumenthal, L. A., Busch, G. T., Broeren, A. P., and Bragg, M. B., "Issues in Ice Accretion Simulation on a Subscale Model," AIAA Paper 2006-0262, Jan. 2006.

[26] McCullough, G. B., and Gault, D. E., "Examples of Three Representative Types of Airfoil-Section Stall at Low Speed," NACA TN-2502, Sept. 1951.

[27] Morgan, H. L., Ferris, J. C., and McGhee, R. J., "A Study of High-Lift Airfoils at High Reynolds Numbers in the NASA Langley Low-Turbulence Pressure Tunnel," NASA TM-89125, 1987.